RESEARCH ARTICLE

QUANTUM SIMULATION

Quantum gas microscopy of Kardar-Parisi-Zhang superdiffusion

David Wei[1,2], Antonio Rubio-Abadal[1,2]†, Bingtian Ye[3], Francisco Machado[3,4], Jack Kemp[3], Kritsana Srakaew[1,2], Simon Hollerith[1,2], Jun Rui[1,2]‡, Sarang Gopalakrishnan[5,6], Norman Y. Yao[3,4], Immanuel Bloch[1,2,7], Johannes Zeiher[1,2]*

The Kardar-Parisi-Zhang (KPZ) universality class describes the coarse-grained behavior of a wealth of classical stochastic models. Surprisingly, KPZ universality was recently conjectured to also describe spin transport in the one-dimensional quantum Heisenberg model. We tested this conjecture by experimentally probing transport in a cold-atom quantum simulator via the relaxation of domain walls in spin chains of up to 50 spins. We found that domain-wall relaxation is indeed governed by the KPZ dynamical exponent $z = 3/2$ and that the occurrence of KPZ scaling requires both integrability and a nonabelian SU(2) symmetry. Finally, we leveraged the single-spin–sensitive detection enabled by the quantum gas microscope to measure an observable based on spin-transport statistics. Our results yield a clear signature of the nonlinearity that is a hallmark of KPZ universality.

In many-particle systems, hydrodynamics (*1*, *2*) naturally emerges upon coarse graining from the microscopic equations of motion in both classical and quantum systems (*3*–*7*). A celebrated example of the emergence of hydrodynamics is the so-called Kardar-Parisi-Zhang (KPZ) equation, which governs an abundance of disparate phenomena ranging from interface growth to the shapes of polymers, the spreading of sound waves in fluids, and the growth of entanglement in random quantum circuits (*8*–*11*). A single equation can describe so many distinct physical systems because of the notion of universality (*12*). Indeed, the physical properties of systems described by the KPZ equation follow scaling functions that were exactly computed in a milestone mathematical achievement (*13*). All of these canonical KPZ systems share the feature that their dynamics is highly robust: KPZ scaling requires no particular symmetries and occurs in the presence of external noise (*14*).

Recent efforts have focused on the prediction that KPZ hydrodynamics should emerge in an entirely distinct setting: the spin-½ quantum Heisenberg chain at infinite temperature (*15*–*21*). The appearance of KPZ scaling in such a quantum spin chain is a surprise because the chains lack the properties shared by all canonical KPZ systems. In particular, noise is absent and the KPZ scaling is fragile—it requires integrability (*6*, *22*–*24*), a feature of the Heisenberg spin chain that does not apply to canonical examples of KPZ. The very appearance of nontrivial dynamical scaling in high-temperature near-equilibrium states is unexpected: The theory of dynamical critical phenomena (*25*) does not apply because high-temperature states are far from any equilibrium critical point. Moreover, nonlinear hydrodynamics predicts that transport in spin chains at nonzero temperature should be diffusive (*26*).

Notably, recent conjectures suggest that the emergence of KPZ hydrodynamics in quantum many-body systems could be substantially more general and may apply to any integrable model that exhibits nonabelian symmetry (*27*, *28*), suggesting a fundamental difference from the mechanisms of canonical KPZ (*21*, *27*–*31*). To date, a full theory of KPZ hydrodynamics in the Heisenberg model remains elusive (*26*, *32*). In light of these questions, experimental characterization of the anomalous dynamical exponents of spin transport has been the subject of widespread effort (*33*–*36*). However, because a superdiffusive exponent can arise from a number of distinct microscopic origins (*37*), it is essential to characterize a system beyond the dynamical exponent to establish its hydrodynamical universality class.

In this work, we explore the superdiffusive dynamics of the ferromagnetic Heisenberg model by using a quantum gas microscope with single-site resolution and single-spin–sensitive detection in spin chains of up to 50 spins. Our main results are threefold. First, we observe superdiffusive spin transport with the dynamical exponent $z = 3/2$, consistent with KPZ hydrodynamics. Second, we demonstrate that both integrability and nonabelian symmetry are essential for observing superdiffusion: Breaking integrability by tuning dimensionality restores diffusion, and breaking the symmetry by preparing an initial state with net magnetization leads to ballistic transport (Fig. 1A). Finally, leveraging the ability of our experimental setup to detect spin-resolved snapshots of the entire sample, we map the shot-to-shot dynamical fluctuations (i.e., the "full counting statistics") of the magnetization. These fluctuations carry clear signatures of the intrinsic nonlinearity associated with KPZ hydrodynamics (*38*) and distinguish it from other potential mechanisms for superdiffusion, such as Lévy flights (*26*).

Experimental system

In our experiment, we probed the transport dynamics of bosonic ^{87}Rb atoms trapped in an optical lattice; the atoms occupy the two hyperfine ground states $|\uparrow\rangle = |F = 1, m_F = -1\rangle$ and $|\downarrow\rangle = |F = 2, m_F = -2\rangle$ (where F is the total angular momentum and m_F is the Zeeman sublevel), and their dynamics are captured by a two-species Bose-Hubbard model with on-site interaction U and tunnel coupling $\tilde{t}$. At unit filling and in the limit of strong interactions, the direct tunneling between lattice sites is suppressed, and spin dynamics occur via second-order spin-exchange. The system can be mapped to the spin-½ XXZ model for $|\uparrow\rangle$ and $|\downarrow\rangle$ (*39*, *40*), and, in one dimension, is described by the Hamiltonian

$$\hat{H} = -J\sum_j \left(\hat{S}_j^x\hat{S}_{j+1}^x + \hat{S}_j^y\hat{S}_{j+1}^y + \Delta\hat{S}_j^z\hat{S}_{j+1}^z\right) \quad (1)$$

where Δ quantifies the interaction anisotropy, $J = 4\tilde{t}^2/U$ characterizes the spin-exchange coupling, and j denotes the lattice sites. In our system, the atomic scattering properties yield $\Delta \approx 1$, and the system maps to the isotropic ferromagnetic Heisenberg model (*41*).

We began our experiment by loading a spin-polarized two-dimensional (2D) degenerate gas of ~2000 atoms into a square optical lattice with a spacing of $a = 532$ nm. We achieved a homogeneous box potential over an area of 50 sites by 22 sites by additionally projecting light at a wavelength of 670 nm with a digital micromirror device (DMD), preparing a Mott insulator with a filling of $n_0 = 0.93(1)$ in this box [see details in (*41*)]. Local spin control was realized using light at a wavelength of 787 nm on the DMD (*42*) to apply a site-resolved differential light shift between $|\uparrow\rangle$ and $|\downarrow\rangle$; subsequent microwave driving allowed for local flips of the spatially addressed spins.

[1]Max-Planck-Institut für Quantenoptik, 85748 Garching, Germany. [2]Munich Center for Quantum Science and Technology (MCQST), 80799 Munich, Germany. [3]Department of Physics, University of California, Berkeley, CA 94720, USA. [4]Materials Science Division, Lawrence Berkeley National Laboratory, Berkeley, CA 94720, USA. [5]Department of Physics, The Pennsylvania State University, University Park, PA 16802, USA. [6]Department of Physics and Astronomy, College of Staten Island, Staten Island, NY 10314, USA. [7]Fakultät für Physik, Ludwig-Maximilians-Universität, 80799 Munich, Germany.
*Corresponding author. Email: johannes.zeiher@mpq.mpg.de
†Present address: Institut de Ciències Fotòniques (ICFO), The Barcelona Institute of Science and Technology, 08860 Castelldefels (Barcelona), Spain.
‡Present address: Hefei National Laboratory for Physical Sciences at the Microscale, University of Science and Technology of China, Hefei, Anhui 230026, China.

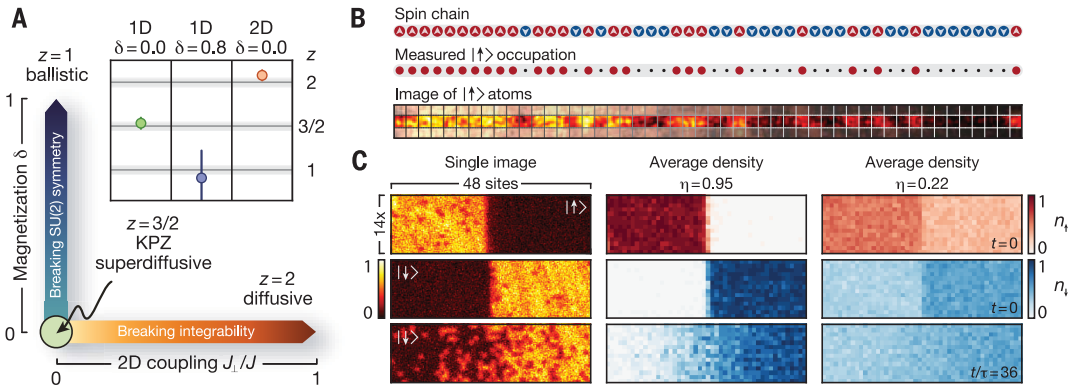

Fig. 1. Hydrodynamic transport in Heisenberg chains and schematic of the experimental system. (**A**) Dynamical exponents for finite-temperature Heisenberg chains. Whereas integrable systems typically display ballistic transport (magnetized chains, $\delta > 0$), nonintegrable systems are generically diffusive (2D Heisenberg model, $J_\perp > 0$). For unmagnetized Heisenberg chains, transport is expected to fall into the KPZ universality class with a superdiffusive exponent $z = 3/2$. (Inset) By measuring polarization transfer $P(t)$ across a domain wall, we directly observe these transport regimes: superdiffusion in the unmagnetized case (green), ballistic transport at finite net magnetization (blue), and diffusion in two dimensions (orange). Exponents are extracted by fitting $P(t) \propto t^{1/z}$; for the ballistic case, we additionally fit a vertical intercept to account for transient initial-time dynamics. Error bars denote SD of the fit. (**B**) In each experimental run, we measure the spin states of a Heisenberg chain (top) by removing one spin species (center) and imaging the atomic site occupation (bottom). (**C**) The Heisenberg chains are achieved in a 2D atomic Mott insulator (analysis region depicted) with controllable interchain coupling. Our setup allows us to prepare domain walls with high-purity η (left and middle columns) and low-purity η (right). We measure the time evolution of both $|\uparrow\rangle$ (top) and $|\downarrow\rangle$ (middle and bottom rows) atoms to extract the polarization transfer.

Such quantum control enabled us to prepare spin domain walls (*16*, *17*, *43*, *44*) by spatially addressing half of the system. Subsequently, we prepared high-entropy states by globally rotating the spins away from the S^z axis by using a resonant microwave pulse and then locally dephasing them by projecting a site-to-site random spin-dependent potential, which we modified from shot to shot (*41*) (Fig. 1C). More precisely, our experiments focused on tracking spin dynamics, starting from a class of initial states containing a spin domain wall with magnetization difference 2η in the middle of the spin chain—i.e., half of the system has magnetization η; the other half has magnetization $-\eta$. In the infinite-temperature limit, $\eta \to 0$, the relaxation of such states yields linear response transport coefficients, as the derivative of the spin profile is precisely the dynamical spin structure factor (*16*, *17*).

To probe 1D spin dynamics in our system, we rapidly quenched the lattice depth along 1D tubes with a length of 50 sites, which suddenly increased the spin-exchange coupling from zero to $J/h = 64(1)\mathrm{s}^{-1}$ (where h is Planck's constant divided by 2π). After tracking the spin dynamics for up to ~45 spin-exchange times $\tau = \hbar/J$, we removed one spin component and measured the remaining occupation via fluorescence imaging (Fig. 1B).

Superdiffusive spin transport

To explore the nature of anomalous spin transport in the 1D Heisenberg model, we initialize the spins in a high-entropy domain-wall state with $\eta = 0.22(2)$. We characterize the subsequent spin transport by measuring the polarization transfer, $P(t)$, defined as the average total number of spins that have crossed the domain wall by time t (*41*). The emergence of hydrodynamics is characterized by the power-law scaling of $P(t) \sim t^{1/z}$ and immediately enables us to extract the underlying dynamical exponent z. As depicted in Fig. 2A, the data exhibit a superdiffusive exponent, $z = 1.54(7)$, consistent with KPZ scaling. By comparison, neither a diffusive ($z = 2$) nor a ballistic ($z = 1$) exponent accurately captures the observed dynamics (Fig. 2B) (*41*). Somewhat surprisingly, we also observe a superdiffusive exponent of $z = 1.45(5)$ upon changing the initial state to a near-pure domain wall with $\eta = 0.95(2)$ (fig. S8) (*26*, *41*, *44*–*46*).

To further explore the superdiffusive dynamics, we investigate the spatially resolved spin profiles at $\eta = 0.22(2)$. Our experimental observations are in quantitative agreement with simulations based on tensor-network numerical techniques (*41*, *46*, *47*) and conform to KPZ dynamics (Fig. 2A). Crucially, when appropriately rescaled by the dynamical exponent, all of the observed spatiotemporal profiles collapse onto a scaling form consistent with the KPZ scaling function (Fig. 2C).

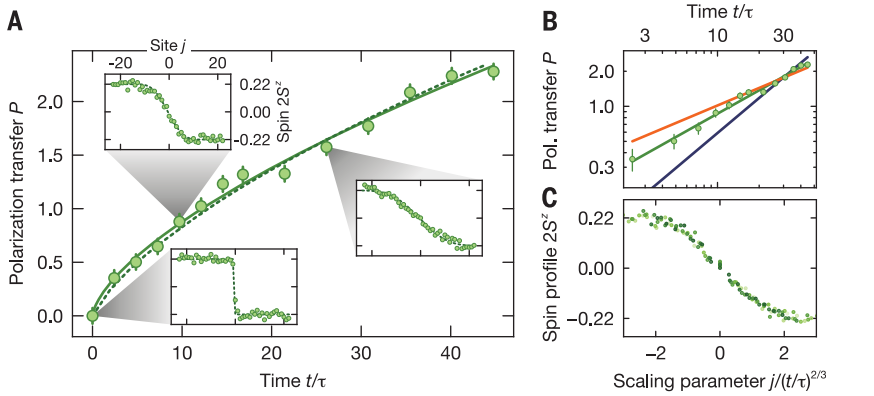

Fig. 2. Superdiffusive spin transport in a high-temperature Heisenberg chain. (**A**) The polarization transfer for a domain-wall initial state with a contrast of $\eta = 0.22(2)$ grows as a power law [$P(t) \propto t^{1/z}$] with a fitted exponent $z = 1.54(7)$ (solid line), indicating superdiffusive transport. The experimental data are consistent with numerical Heisenberg-model simulations (*41*) (dashed line). The insets show the averaged spin profiles $2S_j^z(t)$ at times t/τ = 0, 10, 26, which are compared to simulations (dashed lines). (**B**) Polarization transfer in a double-logarithmic plot. The solid lines are power-law fits with fixed exponents, where a distinction between z = 3/2 (green) and both z = 2 (brown) and z = 1 (blue) is visible. (**C**) When rescaling time by the inverse dynamical exponent, the spatial spin profiles at times t/τ = 5 to 35 (light to dark green) collapse to a characteristic shape consistent with the integrated KPZ function. Error bars denote SEM.

Microscopic origins of superdiffusion

To understand why the combination of integrability and nonabelian symmetry leads to emergent superdiffusive transport, it is instructive to first consider the transport dynamics on

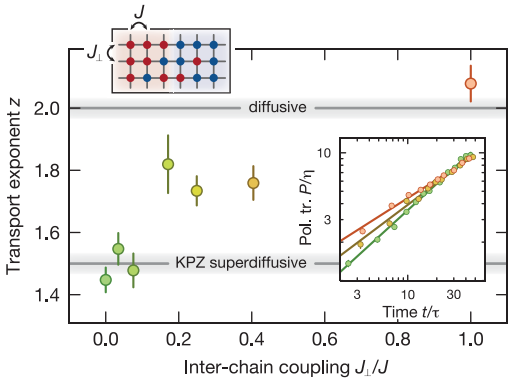

Fig. 3. Evolution toward diffusive transport under a breakdown of integrability. Fitted power-law exponent z for the spin polarization transfer at different coupling strengths between individual 1D chains with initial domain walls with $\eta \approx 0.9$ (*41*). Starting from superdiffusive transport in the purely 1D case, $z = 1.45(5)$, increased interchain coupling breaks the integrability of the system and leads to a crossover toward diffusive transport, reaching $z = 2.08(4)$ in the 2D case, as generically expected for nonintegrable systems. The inset depicts the normalized polarization transfer $P(t)/\eta$ for $J_\perp/J = 0, 0.40(1)$ and $1.00(5)$ (green to orange). Error bars denote SD of the fit.

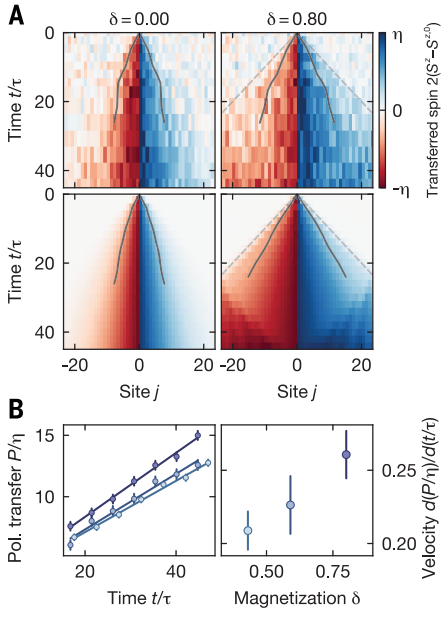

Fig. 4. Ballistic spin dynamics under broken SU(2) symmetry. (**A**) Averaged experimental (top) and numerical (bottom) spin profiles $S_j^z(t)$, from which the initial profile $S_j^{z,0}$ is subtracted. (Left) Unmagnetized low-purity domain wall, $\delta = 0, \eta = 0.22(2)$ (from Fig. 2). Spin transport results from increased spin profile width, which scales with the superdiffusive dynamical exponent. The solid lines indicate the position j where the spin profile crosses $\left|2S_j^z(t) - \delta\right|/\eta = 0.4$; because the profiles themselves are scale invariant, the position of any S^z value follows the z = 3/2 scaling. (Right) Magnetized domain wall, $\delta = 0.80(1), \eta = 0.12(1)$. At the outer edge, the contribution of magnons is visible, transporting spin with the speed of the spin "light cone" (dashed line), which was measured with a quantum walk (*41*). Most of the spin is carried by quasiparticles within the light cone, and thus the width of the profile (solid line) grows faster than in the unmagnetized case. The numerical simulation shows a qualitatively similar behavior. At $t/\tau \simeq 25$ the magnons reach the system edge and are reflected. (**B**) To extract the ballistic polarization-transfer velocity, we linearly fit the normalized polarization transfer after a crossover time, $t/\tau > 16$ (left). We observe transfer velocity growth as the initial domain-wall magnetization δ increases (right, light to dark blue). Error bars denote SD of the fit.

top of a small net magnetization background (*18*–*20*, *48*). In our experiments, this corresponds to preparing domain walls with a finite overall magnetization δ—i.e., half of the system has a magnetization η + δ; the other half has −η + δ. Stable quasiparticles then render spin transport ballistic (Fig. 1A), leading to a characteristic polarization-transfer rate that scales linearly with net magnetization δ (*20*). Even when δ = 0 on average, random local fluctuations of the magnetization will be present; thus, the net magnetization in a typical region of size ℓ will scale as $1/\sqrt{\ell}$. Therefore, the average spin-transport rate across a region of size ℓ also scales as $1/\sqrt{\ell}$, implying that the transport time across the region scales as $\ell/(1/\sqrt{\ell}) \sim \ell^{3/2}$, precisely yielding the KPZ exponent z = 3/2 [see details in (*41*)].

This intuitive analysis suggests two key requirements for superdiffusive transport: (i) integrability ensures the presence of stable quasiparticles that move ballistically, and (ii) the presence of nonabelian SU(2) symmetry makes the characteristic velocity of the ballistic contribution to spin transport vanish. We can experimentally probe these requirements by individually breaking either the integrability or the SU(2) symmetry of the system.

To break integrability, we turn on a finite interchain coupling $J_\perp$ by lowering the lattice depth orthogonal to the 1D spin chains, which effectively causes the system to become 2D (*49*, *50*). We measure the dependence of the polarization transfer on the interchain coupling, starting from an unmagnetized domain wall [$\eta \approx 0.9$ (*41*), δ = 0]. As shown in Fig. 3, the extracted dynamical exponents exhibit a clear flow from superdiffusive transport when $J_\perp = 0$ to diffusive transport, $z = 2.08(4)$, when $J_\perp = J$. Notably, for $J_\perp/J \lesssim 0.1$ integrability is strictly broken, but the transport dynamics remain consistent with superdiffusion within experimentally accessible time scales. This observation bolsters recent theoretical expectations, which suggest that superdiffusion can be particularly robust to perturbations that do not break the nonabelian symmetry (*51*).

Next, we explore the effect of breaking the underlying SU(2) symmetry by using initial states with finite net magnetization δ (*41*). Working with an imbalanced domain-wall initial state [$\eta = 0.12(1), \delta = 0.80(1)$], we observe two main differences from the unmagnetized (δ = 0) case (Fig. 4A). First, the polarization profile exhibits a fast ballistic component that follows the spin "light cone" of the dynamics (with a speed of 1/τ; dashed line in Fig. 4A). This contribution arises from the fastest quasiparticles, which transport spin above the magnetized background (*41*, *52*). Second, within this light cone, polarization spreads substantially faster than in the unmagnetized case; this comprises the bulk of the spin transport and is mediated by slower-moving, net-magnetization–carrying quasiparticles.

At early times, the polarization-transfer dynamics exhibit a superdiffusive power law before crossing over to linear ballistic transport at later times (*41*). In particular, by fitting a power law to the late-time data, $t/\tau > 16$, we extract a dynamical exponent $z = 0.9(3)$, consistent with ballistic spin transport (Fig. 4B). Although our results agree qualitatively with numerical simulations of the Heisenberg model, the magnitude of the measured polarization transfer is smaller; this can be understood as resulting from the presence of hole defects in the initial state (*41*, *53*). In addition to verifying the ballistic nature of the spin dynamics, we can also directly extract the velocity of the underlying quasiparticles. By controlling the overall magnetization of the initial state, we observe the expected increase of the velocity with δ (Fig. 4B), an essential component for understanding the presence of KPZ superdiffusion in spin chains (*20*).

Observing KPZ hydrodynamics

Our previous observations have focused on characterizing superdiffusive spin transport. However, from the perspective of observing KPZ universality, this is insufficient, as multiple different classes of hydrodynamics can exhibit the same dynamical exponent of z = 3/2. To distinguish these classes, we go beyond measurements of the average polarization transfer and analyze the full distribution function of the polarization transfer $\Pr(P; t)$ across snapshots (*38*). This distribution function can distinguish KPZ from potential alternatives

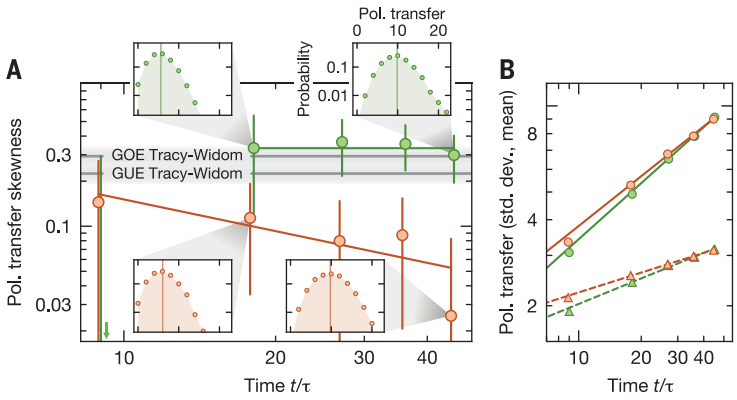

Fig. 5. Distribution function of polarization transfer. (**A**) The probability distribution asymmetry of the polarization transfer expected for KPZ transport is quantified by the skewness. We compare the pure domain-wall dynamics in the 1D case (green) with the nonintegrable 2D case at $J_\perp/J = 0.25(1)$ (orange). Whereas the 2D case becomes symmetric at late times, the 1D distribution remains asymmetric with a skewness of 0.33(8). Gray lines indicate the skewness of the Gaussian-orthogonal-ensemble (GOE) and Gaussian-unitary-ensemble (GUE) Tracy-Widom (TW) distributions (*41*, *54*). Colored lines serve as guides to the eye. (Insets) Probability distributions of the polarization transfer on a logarithmic scale. The vertical line marks the mean of the distribution. (**B**) The mean (circles) of the polarization transfer is consistent with the data shown in Fig. 3 and scales with the power-law (solid lines) exponent [$1/z = 0.67(1)$ in one dimension; $1/z = 0.60(2)$ in two dimensions]. The standard deviation (triangles) features another characteristic transport exponent [the growth exponent (*55*)], which is consistent with the extracted power-law (dashed lines) exponent [$\beta = 0.31(1)$ in one dimension; $\beta = 0.24(1)$ in two dimensions]. Error bars denote the SD obtained from a bootstrap analysis.

such as Lévy flights: For all linear processes (such as Lévy flights or time-rescaled diffusion), the fluctuations of P at late times are necessarily symmetric about the mean; for KPZ, the limiting distribution $\Pr(P; t\to\infty)$ is the Tracy-Widom (TW) distribution (*41*), which is strongly asymmetric (*10*, *54*).

Measuring the statistics of the polarization-transfer distribution therefore gives us a direct experimental observable to discern the underlying hydrodynamical transport equations. This analysis fundamentally relies on the single-shot nature and single-spin sensitivity of our quantum gas microscope. As we measure the occupation of a single-spin species per snapshot, we approximate the polarization-transfer statistics by the statistics for the single-species atom-number transfer, $N_T^{\uparrow(\downarrow)} \approx P/2$, where $N_T^{\uparrow}$ is the number of $|\uparrow\rangle$ atoms on the side of the domain wall initialized with the opposite spin $|\downarrow\rangle$. We quantify the asymmetry of the distribution about its mean $\bar{P}$ by its skewness $(\mu_3(t) - \mu_3(0))/(\mu_2(t) - \mu_2(0))^{3/2}$ (*41*), where $\mu_k(t) = \sum_P (P-\bar{P})^k \Pr(P;t)$ denotes the kth central moment of the distribution.

To begin, we characterize the skewness of the polarization transfer starting from a high-purity domain wall [$\eta = 0.89(1)$, $\delta = 0$] for a 2D geometry with an interchain coupling strength $J_\perp/J = 0.25(1)$. The skewness of the polarization transfer distribution is small overall and is most consistent with a decay toward zero (Fig. 5) (*41*), which corresponds to a fully symmetric distribution and is expected for linear diffusive processes exhibited by the nonintegrable 2D Heisenberg model.

If the 1D Heisenberg model is actually governed by nonlinear KPZ hydrodynamics, one would expect markedly distinctive behavior for the skewness as a function of time. In particular, the nonlinearity of the KPZ equation would lead to a finite skewness, which is constant over time. We indeed observe that the skewness saturates to a finite value of 0.33(8) when starting from an initial state with $\eta = 0.91(2)$ and $\delta = 0$ (Fig. 5). In agreement with numerical simulations, this value is consistent with the skewness of the Gaussian-orthogonal-ensemble (GOE) TW distribution, 0.294 (*54*). Our experiment directly rules out linear transport processes and thus provides a strong indication that transport in the 1D quantum Heisenberg chain is governed by KPZ hydrodynamics.

Discussion and conclusion

Our results support the theoretical conjecture that spin transport in the 1D Heisenberg model belongs to the KPZ universality class, with a superdiffusive transport exponent $z = 3/2$. We have experimentally demonstrated that both integrability and nonabelian symmetry are essential for stabilizing superdiffusive transport. Moreover, we exploit the single-spin sensitivity of our setup to extract the full distribution function of the polarization transfer. This distribution function exhibits a large skewness that does not decay in time, demonstrating that spin transport in this system belongs to a strongly coupled, nonlinear dynamical universality class.

Our work builds and expands on recent experimental explorations of Heisenberg-model spin dynamics. These experiments include neutron scattering studies of the quantum material $KCuF_3$ (*36*), as well as experiments that probe the relaxation of spin-spiral initial states in ultracold gases (*33*–*35*). In the 1D Heisenberg model, the relaxation of such spin-spiral states is nongeneric because they are approximate eigenstates in the long-wavelength limit (*26*). Empirically, spin spirals relax with a diffusive exponent $z = 2$. By considering a more generic family of domain-wall initial states, we are able to directly probe (and controllably move away from) the high-temperature linear-response limit where KPZ transport is thought to occur.

Our results open the door to a number of future directions. First, the discrepancy between the relaxation of domain walls and spin spirals (away from linear response) indicates that relaxation in integrable systems is generally strongly dependent on initial state, although we currently lack a theory of this nonlinear regime. Second, the robustness of our results along the crossover from the Heisenberg to the (nonintegrable) Bose-Hubbard regime remains to be fully understood (*51*). In this context, a comparison between the nonintegrable Bose-Hubbard model and the integrable Fermi-Hubbard model (*53*) could be of particular interest. Finally, the observable we introduced to capture fluctuation effects—namely, the statistics of single shots of the polarization transfer—promises to be a powerful diagnostic tool for new phases of interacting quantum systems. A theory of this quantity already exists for the KPZ universality class, but developing a more general theory of such transport fluctuations will be an important task for future theoretical work.

Note added in proof: During the completion of this manuscript, we became aware of related work to observe superdiffusive transport in a long-range interacting ion chain (*37*).

REFERENCES AND NOTES

1. H. Spohn, *Large Scale Dynamics of Interacting Particles* (Springer, 2012).
2. G. Birkhoff, *Hydrodynamics* (Princeton Univ. Press, 2015).
3. R. E. Wyatt, *Quantum Dynamics with Trajectories: Introduction to Quantum Hydrodynamics*, vol. 28 (Springer, 2006).
4. S. Mukerjee, V. Oganesyan, D. Huse, *Phys. Rev. B* **73**, 035113 (2006).
5. L. Erdős, B. Schlein, H.-T. Yau, *Phys. Rev. Lett.* **98**, 040404 (2007).
6. O. A. Castro-Alvaredo, B. Doyon, T. Yoshimura, *Phys. Rev. X* **6**, 041065 (2016).
7. C. Zu *et al.*, *Nature* **597**, 45–50 (2021).
8. M. Kardar, G. Parisi, Y.-C. Zhang, *Phys. Rev. Lett.* **56**, 889–892 (1986).
9. T. Halpin-Healy, K. Takeuchi, *J. Stat. Phys.* **160**, 794–814 (2015).
10. H. Spohn, *J. Stat. Mech.* **2020**, 044001 (2020).
11. A. Nahum, J. Ruhman, S. Vijay, J. Haah, *Phys. Rev. X* **7**, 031016 (2017).
12. L. P. Kadanoff, *Physica A* **163**, 1–14 (1990).
13. M. Prähofer, H. Spohn, *J. Stat. Phys.* **115**, 255–279 (2004).

14. M. Gubinelli, N. Perkowski, *Commun. Math. Phys.* **349**, 165–269 (2017).
15. M. Znidarič, *Phys. Rev. Lett.* **106**, 220601 (2011).
16. M. Ljubotina, M. Žnidarič, T. Prosen, *Nat. Commun.* **8**, 16117 (2017).
17. M. Ljubotina, M. Žnidarič, T. Prosen, *Phys. Rev. Lett.* **122**, 210602 (2019).
18. S. Gopalakrishnan, R. Vasseur, *Phys. Rev. Lett.* **122**, 127202 (2019).
19. J. De Nardis, M. Medenjak, C. Karrasch, E. Ilievski, *Phys. Rev. Lett.* **123**, 186601 (2019).
20. S. Gopalakrishnan, R. Vasseur, B. Ware, *Proc. Natl. Acad. Sci. U.S.A.* **116**, 16250–16255 (2019).
21. V. B. Bulchandani, *Phys. Rev. B* **101**, 041411 (2020).
22. B. Bertini, M. Collura, J. De Nardis, M. Fagotti, *Phys. Rev. Lett.* **117**, 207201 (2016).
23. E. Ilievski, J. De Nardis, *Phys. Rev. Lett.* **119**, 020602 (2017).
24. V. B. Bulchandani, R. Vasseur, C. Karrasch, J. E. Moore, *Phys. Rev. B* **97**, 045407 (2018).
25. P. C. Hohenberg, B. I. Halperin, *Rev. Mod. Phys.* **49**, 435–479 (1977).
26. V. B. Bulchandani, S. Gopalakrishnan, E. Ilievski, *J. Stat. Mech.* **2021**, 084001 (2021).
27. Ž. Krajnik, T. Prosen, *J. Stat. Phys.* **179**, 110–130 (2020).
28. E. Ilievski, J. De Nardis, S. Gopalakrishnan, R. Vasseur, B. Ware, *Phys. Rev. X* **11**, 031023 (2021).
29. T. Prosen, B. Zunkovič, *Phys. Rev. Lett.* **111**, 040602 (2013).
30. A. Das, M. Kulkarni, H. Spohn, A. Dhar, *Phys. Rev. E* **100**, 042116 (2019).
31. Ž. Krajnik, E. Ilievski, T. Prosen, *SciPost Phys.* **9**, 038 (2020).
32. B. Bertini *et al*., *Rev. Mod. Phys.* **93**, 025003 (2021).
33. S. Hild *et al*., *Phys. Rev. Lett.* **113**, 147205 (2014).
34. P. N. Jepsen *et al*., *Nature* **588**, 403–407 (2020).
35. P. N. Jepsen *et al*., *Phys. Rev. X* **11**, 041054 (2021).
36. A. Scheie *et al*., *Nat. Phys.* **17**, 726–730 (2021).
37. M. K. Joshi *et al*., *Science* **376**, 720–724 (2022).
38. A. K. Hartmann, P. Le Doussal, S. N. Majumdar, A. Rosso, G. Schehr, *Europhys. Lett.* **121**, 67004 (2018).
39. L.-M. Duan, E. Demler, M. D. Lukin, *Phys. Rev. Lett.* **91**, 090402 (2003).
40. A. B. Kuklov, B. V. Svistunov, *Phys. Rev. Lett.* **90**, 100401 (2003).
41. See supplementary materials.
42. T. Fukuhara *et al*., *Nat. Phys.* **9**, 235–241 (2013).
43. J. C. Halimeh, A. Wöllert, I. McCulloch, U. Schollwöck, T. Barthel, *Phys. Rev. A* **89**, 063603 (2014).
44. G. Misguich, K. Mallick, P. L. Krapivsky, *Phys. Rev. B* **96**, 195151 (2017).
45. O. Gamayun, Y. Miao, E. Ilievski, *Phys. Rev. B* **99**, 140301 (2019).
46. B. Ye, F. Machado, C. D. White, R. S. K. Mong, N. Y. Yao, *Phys. Rev. Lett.* **125**, 030601 (2020).
47. C. D. White, M. Zaletel, R. S. K. Mong, G. Refael, *Phys. Rev. B* **97**, 035127 (2018).
48. J. De Nardis, S. Gopalakrishnan, E. Ilievski, R. Vasseur, *Phys. Rev. Lett.* **125**, 070601 (2020).
49. Y. Tang *et al*., *Phys. Rev. X* **8**, 021030 (2018).
50. M. A. Nichols *et al*., *Science* **363**, 383–387 (2019).
51. J. De Nardis, S. Gopalakrishnan, R. Vasseur, B. Ware, *Phys. Rev. Lett.* **127**, 057201 (2021).
52. F. Weiner, P. Schmitteckert, S. Bera, F. Evers, *Phys. Rev. B* **101**, 045115 (2020).
53. M. Fava, B. Ware, S. Gopalakrishnan, R. Vasseur, S. A. Parameswaran, *Phys. Rev. B* **102**, 115121 (2020).
54. M. Prähofer, H. Spohn, *Phys. Rev. Lett.* **84**, 4882–4885 (2000).
55. F. Family, T. Vicsek, *J. Phys. Math. Gen.* **18**, L75–L81 (1985).
56. D. Wei *et al*., Quantum gas microscopy of Kardar-Parisi-Zhang superdiffusion, version 1.0, Edmond (2022); https://doi.org/10.17617/3.8w.

ACKNOWLEDGMENTS

We gratefully acknowledge discussions with J. Moore, R. Vasseur, and M. Zaletel. We thank K. Takeuchi, T. Prosen, and H. Spohn for comments on the manuscript. **Funding:** We acknowledge funding from the Max Planck Society (MPG), the European Union (PASQuanS grant no. 817482), and the Deutsche Forschungsgemeinschaft (DFG, German Research Foundation) under Germany's Excellence Strategy – EXC-2111 – 390814868. B.Y., F.M., J.K., and N.Y.Y. acknowledge support from the ARO (grant no. W911NF-21-1-0262) and through the MURI program (W911NF-20-1-0136). J.R. acknowledges funding from the Max Planck Harvard Research Center for Quantum Optics. S.G. acknowledges support from the NSF (DMR-1653271). N.Y.Y. acknowledges support from the David and Lucile Packard Foundation and the W. M. Keck Foundation. **Author contributions:** All authors contributed substantially to the work presented in this manuscript. D.W., A.R.-A., K.S., and S.H. acquired the data and maintained the experimental apparatus. D.W. analyzed the data. B.Y., F.M., J.K., S.G., and N.Y.Y. performed the numerical and analytical calculations. I.B. and J.Z. supervised the study. All authors worked on the interpretation of the data and contributed to writing the manuscript. **Competing interests:** The authors declare no competing interests. **Data and materials availability:** The data shown in the main text and supplementary materials and the code associated with the numerical simulations are available from the Edmond repository of the Max Planck Society (*56*).

SUPPLEMENTARY MATERIALS

science.org/doi/10.1126/science.abk2397
Supplementary Text
Figs. S1 to S18
Tables S1 and S2
References (*57*–*63*)

Submitted 30 June 2021; accepted 10 March 2022
10.1126/science.abk2397